



A FULLY SELF-CONSISTENT MULTI-LAYERED MODEL OF JUPITER

DALI KONG^{1,2}, KEKE ZHANG^{2,3}, AND GERALD SCHUBERT⁴

¹ Key Laboratory of Planetary Sciences, Shanghai Astronomical Observatory, Chinese Academy of Sciences, Shanghai 200030, China; D.Kong@exeter.ac.uk
² Center for Geophysical and Astrophysical Fluid Dynamics, College of Engineering, Mathematics and Physical Sciences, University of Exeter, Exeter, EX4 4QF, UK

³ Lunar and Planetary Science Laboratory, Macau University of Science and Technology, Macau, China; K.Zhang@exeter.ac.uk

⁴ Department of Earth, Planetary, and Space Sciences, University of California, Los Angeles, CA 90095-1567, USA; schubert@ucla.edu

Received 2016 March 9; revised 2016 May 8; accepted 2016 May 23; published 2016 July 27

ABSTRACT

We construct a three-dimensional, fully self-consistent, multi-layered, non-spheroidal model of Jupiter consisting of an inner core, a metallic electrically conducting dynamo region, and an outer molecular electrically insulating envelope. We assume that the Jovian zonal winds are on cylinders parallel to the rotation axis but, due to the effect of magnetic braking, are confined within the outer molecular envelope. We also assume that the location of the molecular-metallic interface is characterized by its equatorial radius HR_e , where R_e is the equatorial radius of Jupiter at the 1 bar pressure level and H is treated as a parameter of the model. We solve the relevant mathematical problem via a perturbation approach. The leading-order problem determines the density, size, and shape of the inner core, the irregular shape of the 1 bar pressure level, and the internal structure of Jupiter that accounts for the full effect of rotational distortion, but without the influence of the zonal winds; the next-order problem determines the variation of the gravitational field solely caused by the effect of the zonal winds on the rotationally distorted non-spheroidal Jupiter. The leading-order solution produces the known mass, the known equatorial and polar radii, and the known zonal gravitational coefficient J_2 of Jupiter within their error bars; it also yields the coefficients J_4 and J_6 within about 5% accuracy, the core equatorial radius $0.09R_e$ and the core density $\rho_c = 2.0 \times 10^4 \text{ kg m}^{-3}$ corresponding to 3.73 Earth masses; the next-order solution yields the wind-induced variation of the zonal gravitational coefficients of Jupiter.

Key words: gravitation – planets and satellites: individual (Jupiter) – planets and satellites: interiors

1. INTRODUCTION

The *Juno* spacecraft, now on its way to Jupiter, will make high-precision measurements of the gravitational field of the giant planet (Kaspi et al. 2010). While the first three zonal gravitational coefficients J_2, J_4, J_6 are at present accurately measured (Jacobson 2003), the *Juno* spacecraft will carry out high-precision measurements of the gravitational coefficients up to J_{12} (Bolton 2005). Interpretation of these measurements requires an accurate description of the shape and internal structure of Jupiter in its equilibrium state under the balance of self-gravity, internal pressure, and strong rotational effects as well as under the influence of the fast zonal winds. The primary purpose of this study is to construct an accurate model of Jupiter for such interpretation.

The interpretation involves the highly accurate solution of two different but inseparable problems. The first problem is concerned with an accurate description of the shape and internal density profile of Jupiter for which the effect of rotational distortion cannot be treated as a small perturbation on a spherically symmetric state. Kong et al. (2013b) proposed a hybrid inverse numerical method, via a finite-element formulation, for calculating the shape and internal structure of a rapidly rotating gaseous body valid for arbitrary angular velocity Ω . For numerical convenience, this inverse method makes an assumption that the outer bounding surface of the body is in the shape of an oblate spheroid. While the spheroidal-shape approximation has only small effects on the lower-order gravitational coefficients such as J_2 , the small-scale density variation resulting from the non-spheroidal shape can make a substantial contribution to the high-order gravitational coefficients J_n with $n \geq 10$ (Kong et al. 2015). Hubbard (2013) developed a radially discontinuous numerical method, which,

because of the convergence radius of the expansion (Hubbard et al. 2014), is valid only for moderate angular velocity Ω but applicable to all giant planets in the solar system. By dividing a rotating body into a number of concentric incompressible layers within which the density is assumed constant, Hubbard (2013) iterated over the shapes of the concentric layers until all the interfaces became equipotential surfaces.

The second problem is concerned with an accurate description of the variation of the zonal gravitational coefficients $\Delta J_2, \Delta J_4, \dots, \Delta J_{12}$ caused by the effect of the Jovian zonal winds. On the basis of the assumptions that the rotational effect upon the Jovian shape is negligibly small and that the observed cloud-level zonal winds extend on the cylinders, but decay exponentially in the radial direction, Kaspi et al. (2010) solved the thermal-wind equation to estimate the wind-induced density anomaly and the corresponding gravitational correction ΔJ_n with n even and $n \geq 2$. By assuming that Jupiter is in the shape of an oblate spheroid and that the observed cloud-level zonal winds extend all the way on the cylinders from the northern to the southern hemisphere without being blocked by the Jovian magnetic field, Kong et al. (2013a) computed the variation of the Jovian gravitational coefficients $\Delta J_2, \Delta J_4, \dots, \Delta J_{12}$ caused by the effect of the zonal winds, while Kong et al. (2014) revealed the dominance of the equatorial zonal jets in determining the high-order gravitational coefficients. Furthermore, the Jovian magnetic field is generated by convection-driven motion in its deep metallic region that must be non-axisymmetric, but whose amplitude and structure are unknown; Kong et al. (2016) discussed a promising way of probing the Jovian convective dynamo via its effect on the external non-axisymmetric gravitational field.

In comparison to our previous studies (Kong et al. 2013a, 2013b), there exist five major methodical advantages/

differences of the present work, representing a significant step toward building a physically realistic and computationally accurate model of Jupiter. First, the spheroidal-shape approximation (Kong et al. 2013b)—which assumes the outer bounding surface of Jupiter is in the shape of an oblate spheroid—is completely removed. In the present study, the shape of the bounding surface is geometrically irregular and determined fully self-consistently by the required equilibrium condition. Second, an inner core is introduced to the previous single-layered model (Kong et al. 2013b) and the shape and mass of the inner core are also determined self-consistently as a solution of the coupled, multi-layered system. Third, the computationally convenient zero-pressure boundary condition at the outer bounding surface (Kong et al. 2013b) is, in the present study, replaced by the physically more realistic 1 bar pressure condition. Fourth, the assumption (Kong et al. 2013a, 2014) that the cloud-level zonal winds extend all the way on the cylinders from the northern to the southern hemisphere is also removed. In the present study, the zonal winds are confined between the 1 bar pressure surface and the molecular-metallic interface, and the shape of the 1 bar surface and the interface is geometrically irregular. Fifth, a new parameter H is introduced in the present study to describe the location of the molecular-metallic interface: the equatorial radius of the interface is given by HR_e , where R_e is the equatorial radius of Jupiter at the 1 bar pressure level. Compared to the single-layer model (Kong et al. 2013a, 2013b), the present fully self-consistent, multi-layered model is physically more realistic because an inner core is likely to exist according to the interior models of Jupiter (Stevenson 1982; Guillot 2005) and because the cloud-level zonal winds extend undiminished on cylinders only to the molecular-metallic interface where the effect of magnetic braking (Liu et al. 2008) would stop their penetration, a scenario consistent with existing Jovian dynamic models (Heimpel et al. 2005; Gastine & Wicht 2012; Jones & Kuzanyan 2012).

In what follows, we begin by presenting the multi-layered model of Jupiter and the related governing equations in Section 2 followed by a discussion of the perturbation method in Section 3. The results of the multi-layered model are discussed in Section 4 with a summary and some remarks given in Section 5.

2. MODEL

Following existing Jovian interior models (Stevenson 1982; Guillot 2005; Helled et al. 2011; Nettelmann et al. 2012; Hubbard & Militzer 2016), our multi-layered model of Jupiter consists of three major parts: a rocky inner core, a metallic region where the Jovian magnetic field is generated by its convective dynamo, and an outer molecular insulating envelope where the observed cloud-level zonal winds originate. A sketch of the multi-layered Jovian model is illustrated in Figure 1. We assume that the zonal winds, because of the effect of magnetic braking, cannot penetrate into the dynamo region. Exterior to the inner core, the density ρ of the fully compressible barotropic fluid is assumed to be a function only of the pressure p obeying the polytropic law with an index of unity

$$p = K \rho^{1+1/n}, \quad (1)$$

where $n = 1$ and K are constants. The polytropic gas of index unity is believed to provide a reasonably good approximation

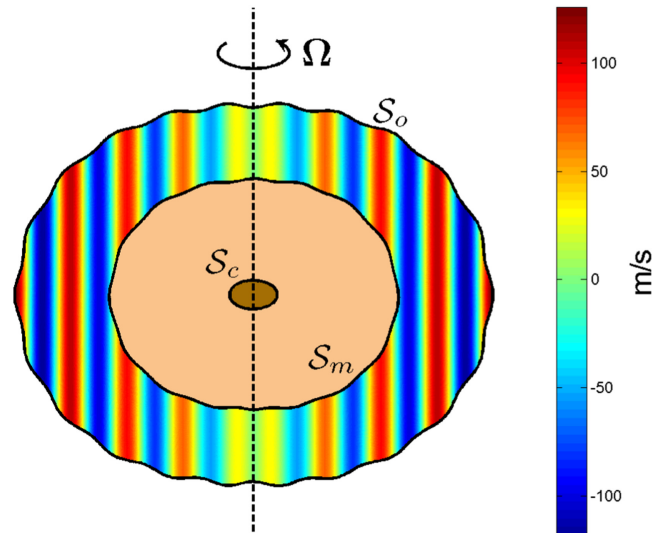


Figure 1. Sketch of the three-layer Jovian model in a meridional plane: a small rocky core, a metallic hydrogen–helium dynamo region and an outer molecular insulating envelope. Three surfaces characterize the model: the core-metallic interface S_c , the molecular-metallic interface S_m and the outer 1 bar pressure surface S_o . The Jovian zonal winds are assumed to be on cylinders parallel to the rotation axis and confined between S_m and S_o .

for Jupiter’s interior (Hubbard 1999). Geometrically, there are three surfaces that characterize the multi-layered model: the core-metallic interface S_c , the molecular-metallic interface S_m and the outer 1 bar pressure surface S_o , which are depicted in Figure 1. The three surfaces are to be determined self-consistently without making any prior assumptions about their shape. For the convenience of discussion, the region surrounded by S_c is denoted by \mathcal{D}_c , the domain enclosed between S_m and S_o is denoted by \mathcal{D}_m and the domain enclosed between S_c and S_o is denoted by \mathcal{D}_o .

Our model also assumes that (1) the convective flow in the metallic dynamo region is dominated by the non-axisymmetric small scale and, hence, its contribution to the zonal gravitational coefficient J_n is negligible; (2) the Rossby number associated with the Jovian zonal winds is small and viscous forces are much smaller than Coriolis forces; (3) the zonal winds are in a statistically steady state and confined between the molecular-metallic interface S_m and the 1 bar pressure surface S_o ; (4) contribution from the mass beyond the 1 bar pressure surface S_o is negligibly small; and (5) Jupiter is isolated, rotating rapidly with the uniform angular velocity $\hat{z}\Omega_J$. The above assumptions lead to the following governing equations for the fluid region \mathcal{D}_o in the rotating frame of reference:

$$2\Omega_J \hat{z} \times \mathbf{u}_0 = -\frac{1}{\rho} \nabla p - \nabla V + \frac{\Omega_J^2}{2} \nabla |\hat{z} \times \mathbf{r}|^2, \quad (2)$$

$$\nabla^2 V = 4\pi G \rho, \quad (3)$$

$$p = K \rho^2, \quad (4)$$

$$\nabla \cdot (\mathbf{u}_0 \rho) = 0, \quad (5)$$

where \mathbf{u}_0 denotes the zonal winds on cylinders parallel to the rotation axis confined within the outer molecular layer \mathcal{D}_m , \mathbf{r} denotes the position vector with its origin at the center of figure, $p(\mathbf{r})$ is the pressure and $\rho(\mathbf{r})$ is the density in the region

\mathcal{D}_o , and $V(\mathbf{r})$ is the gravitational potential with $G = 6.67384 \times 10^{-11} \text{ m}^3 \text{ kg}^{-1} \text{ s}^{-2}$, the universal gravitational constant. Equations (2)–(5) are solved subject to the two boundary conditions

$$[p]_{|r|=\mathcal{S}_o} = 1 \text{ bar}, \quad (6)$$

$$G \left[\int \int \int_{\mathcal{D}_c} \frac{\rho_c d^3 \mathbf{r}'}{|\mathbf{r} - \mathbf{r}'|} + \int \int \int_{\mathcal{D}_o} \frac{\rho(\mathbf{r}') d^3 \mathbf{r}'}{|\mathbf{r} - \mathbf{r}'|} + \frac{\Omega_J^2}{2} |\hat{\mathbf{z}} \times \mathbf{r}|^2 \right]_{|r|=\mathcal{S}_o} = \text{constant}, \quad (7)$$

where $[\mathcal{F}]_{|r|=\mathcal{S}_o}$ denotes the evaluation of a function \mathcal{F} at the 1 bar pressure surface \mathcal{S}_o that is not only irregular but also a priori unknown, Equation (7) requires the surface \mathcal{S}_o to be equipotential and $\int \int \int_{\mathcal{D}} d^3 \mathbf{r}'$ represents the volume integration over the domain \mathcal{D} .

For a given zonal wind \mathbf{u}_o in \mathcal{D}_m and an initial guess for the inner core properties, Equations (2)–(5) are solved, via an iterative scheme, for determining the core-metallic interface \mathcal{S}_c , the core density ρ_c and the density profile $\rho(\mathbf{r})$ in \mathcal{D}_o , and the 1 bar pressure surface \mathcal{S}_o that satisfy the boundary conditions (6)–(7). The external gravitational potential $V(\mathbf{r})$ can be then obtained by carrying out the three-dimensional integration in the irregular domain bounded by the surface \mathcal{S}_o ,

$$V(\mathbf{r}) = -G \left[\int \int \int_{\mathcal{D}_c} \frac{\rho_c d^3 \mathbf{r}'}{|\mathbf{r} - \mathbf{r}'|} + \int \int \int_{\mathcal{D}_o} \frac{\rho(\mathbf{r}') d^3 \mathbf{r}'}{|\mathbf{r} - \mathbf{r}'|} \right], \quad |r| \geq R_e, \quad (8)$$

which can then be projected onto an expansion in terms of Legendre functions P_n ,

$$V(\mathbf{r}) = -\frac{GM_J}{r} \left[1 - \sum_{n=2}^{\infty} J_n \left(\frac{R_e}{r} \right)^n P_n(\cos \theta) \right], \quad r \geq R_e, \quad (9)$$

where M_J is Jupiter's mass enclosed by the 1 bar pressure surface \mathcal{S}_o , n takes even integers, (r, θ, ϕ) are spherical polar coordinates with $\theta = 0$ at the axis of rotation, and J_2, J_4, J_6, \dots , are the zonal gravitational coefficients.

3. METHODS

Since the speed of the Jovian zonal winds is much smaller than its rigid-body rotation, Equations (2)–(5) subject to the boundary conditions (6)–(7) can be solved by a perturbation method making use of the expansions

$$p(\mathbf{r}) = p_0(\mathbf{r}) + p'(\mathbf{r}), \quad (10)$$

$$\rho(\mathbf{r}) = \rho_0(\mathbf{r}) + \rho'(\mathbf{r}), \quad (11)$$

$$J_n = (J_n)_0 + \Delta J_n, \quad (12)$$

$$V(\mathbf{r}) = V_0(\mathbf{r}) + V'(\mathbf{r}), \quad (13)$$

where the leading-order solution, $[p_0(\mathbf{r}), \rho_0(\mathbf{r}), V_0(\mathbf{r}), (J_n)_0]$, represents a hydrostatic state that accounts for the effect of rotational distortion, but is unaffected by the zonal winds, and the next-order solution, $[p'(\mathbf{r}), \rho'(\mathbf{r}), V'(\mathbf{r}), \Delta J_n]$ denotes perturbations arising from the effect of the zonal winds confined within the molecular envelope \mathcal{D}_m . It should be stressed that the perturbation method yields two problems that

are mathematically and physically coupled. The leading-order problem determines the inner core properties, the 1 bar pressure surface \mathcal{S}_o , and the internal density distribution $\rho_0(\mathbf{r})$ in \mathcal{D}_o , while the next-order problem determines the density perturbation $\rho'(\mathbf{r})$ in the region enclosed by \mathcal{S}_m and \mathcal{S}_o .

Substitution of the expansions into Equations (2)–(5) yields the leading-order problem governed by

$$\frac{1}{\rho_0} \nabla p_0 = -\nabla V_0 + \frac{\Omega_J^2}{2} \nabla |\hat{\mathbf{z}} \times \mathbf{r}|^2, \quad (14)$$

$$\nabla^2 V_0 = 4\pi G \rho_0, \quad (15)$$

$$p_0 = K \rho_0^2, \quad (16)$$

subject to the two boundary conditions

$$[p_0]_{|r|=\mathcal{S}_o} = 1 \text{ bar}, \quad (17)$$

$$G \left[\int \int \int_{\mathcal{D}_c} \frac{\rho_c d^3 \mathbf{r}'}{|\mathbf{r} - \mathbf{r}'|} + \int \int \int_{\mathcal{D}_o} \frac{\rho_0(\mathbf{r}') d^3 \mathbf{r}'}{|\mathbf{r} - \mathbf{r}'|} + \frac{\Omega_J^2}{2} |\hat{\mathbf{z}} \times \mathbf{r}|^2 \right]_{|r|=\mathcal{S}_o} = \text{constant}, \quad (18)$$

at the 1 bar pressure surface \mathcal{S}_o of Jupiter.

A three-dimensional finite-element method is employed to solve Equations (14)–(16) fully self-consistently subject to the two boundary conditions (17)–(18) without making any prior assumptions. For the purpose of describing the 1 bar pressure surface \mathcal{S}_o of Jupiter, it is mathematically convenient to adopt oblate spheroidal coordinates (ξ, η, ϕ) , which are defined by the coordinate transformation with cartesian coordinates

$$x = 0.35421 R_e \sqrt{(1 + \xi^2)(1 - \eta^2)} \cos \phi, \quad (19)$$

$$y = 0.35421 R_e \sqrt{(1 + \xi^2)(1 - \eta^2)} \sin \phi, \quad (20)$$

$$z = 0.35421 R_e \xi \eta, \quad (21)$$

where $R_e = 71492 \text{ km}$ is the equatorial radius of Jupiter at the 1 bar pressure level, $\xi = \text{constant}$ represents a confocal oblate spheroid, and $\eta = \text{constant}$ describes confocal hyperboloids. When defining oblate spheroidal coordinates (ξ, η, ϕ) , the scaling factor $0.35421 R_e$ in the coordinate transformation (19)–(21) is largely arbitrary and does not affect the final solution. With oblate spheroidal coordinates, the 1 bar pressure surface \mathcal{S}_o of Jupiter can always be described by the expansion

$$\xi_{\text{1bar-surface}} = \xi_0 + \sum_{m=0}^{\infty} \sum_{n=1}^{\infty} [h_n^m \tilde{P}_n^m(\eta) \cos m\phi + g_n^m \tilde{P}_n^m(\eta) \sin m\phi], \quad (22)$$

where $-1 \leq \eta \leq 1$, $0 \leq \phi < 2\pi$, ξ_0 and h_n^m and g_n^m are coefficients to be determined and $\tilde{P}_l^m(\eta)$ are the associated Legendre polynomials normalized by

$$\int_{-1}^1 \tilde{P}_l^m(\eta) \tilde{P}_j^m(\eta) d\eta = \delta_{lj};$$

for instance, we have

$$\tilde{P}_2^0(\eta) = \sqrt{\frac{5}{8}} (3\eta^2 - 1),$$

$$\tilde{P}_4^0(\eta) = \sqrt{\frac{9}{128}} (35\eta^4 - 30\eta^2 + 3).$$

Because of the completeness of the spheroidal Legendre polynomials $\tilde{P}_l^m(\eta)$, expression (22) can, in principle, be used to describe the arbitrary shape of any rapidly rotating gaseous planets. Our three-dimensional method is valid for any $|h_n^m|$ and $|g_n^m|$ in (22) without requiring a small departure from the shape of an oblate spheroid. Moreover, our model does not assume that the shape of a rapidly rotating gaseous body—which would be generally non-axisymmetric ($\partial/\partial\phi \neq 0$)—is axisymmetric ($\partial/\partial\phi = 0$). In the case with Jupiter’s parameters, however, it turns out that the three-dimensional solution is always axisymmetric, i.e., $h_n^m = 0$ with $m \geq 1$ and $g_n^m = 0$ with $m \geq 0$ in (22), and that the shape of the 1 bar pressure surface \mathcal{S}_o differs only slightly from the shape of an oblate spheroid, i.e., ξ_0 is dominant in (22) with all other coefficients h_n^0 , $n = 2, 4, \dots$ being small. Our discussion will, hence, concentrate on the values of ξ_0 and non-zero axisymmetric coefficients h_n^0 with even n in (22). After solving Equations (14)–(16) subject to the conditions (17)–(18) and the constraint

$$M_J = \rho_c \iiint_{\mathcal{D}_c} d^3\mathbf{r}' + \iiint_{\mathcal{D}_o} \rho_0(\mathbf{r}') d^3\mathbf{r}', \quad (23)$$

we can determine the core-metallic interface \mathcal{S}_c , the 1 bar pressure surface \mathcal{S}_o , the core density ρ_c , and the density profile $\rho_0(\mathbf{r})$ in \mathcal{D}_o .

The next-order problem, which gives rise to the density anomaly $\rho'(\mathbf{r})$ induced by the zonal winds \mathbf{u}_0 in the molecular region \mathcal{D}_m and the concomitant gravitational potential $V'(\mathbf{r})$, is governed by the equations

$$2\Omega_1 \hat{\mathbf{z}} \times \mathbf{u}_0 = -2K \nabla \rho' - \nabla V', \quad (24)$$

$$\nabla^2 V' = 4\pi G \rho', \quad (25)$$

$$\nabla \cdot (\mathbf{u}_0 \rho_0) = 0, \quad (26)$$

subject to the boundary conditions

$$[\rho'(\mathbf{r})]_{|r|=\mathcal{S}_o} = 0 \quad \text{and} \quad [\rho'(\mathbf{r})]_{|r|=\mathcal{S}_m} = 0, \quad (27)$$

where \mathcal{S}_m denotes a constant density surface between \mathcal{S}_c and \mathcal{S}_o whose equatorial radius is given by HR_e . Note that Equation (26) is automatically satisfied because of the property of the leading-order solution $\rho_0(\mathbf{r})$. In our analysis, the small-shape variation in \mathcal{S}_m and \mathcal{S}_o caused by the effect of the zonal winds is neglected at this order and the location of the molecular-metallic interface \mathcal{S}_m , characterized by the size of H , is treated as a parameter. The first condition at \mathcal{S}_o in (27) is a consequence of both the condition (6) that the outer bounding surface \mathcal{S}_o represents the 1 bar pressure surface and the perturbation expansions (10)–(11); the second condition at \mathcal{S}_m in (27) stems from an assumption that the molecular-metallic interface \mathcal{S}_m represents a constant density surface. The boundary condition (27) is consistent with most thermal convection models in which the isothermal boundary condition—which corresponds to the density perturbation $\rho' = 0$ —is usually adopted. The profile of the zonal winds \mathbf{u}_0 , which are on cylinders parallel to the rotation axis but are confined between \mathcal{S}_m and \mathcal{S}_o as sketched in Figure 1, is uniquely

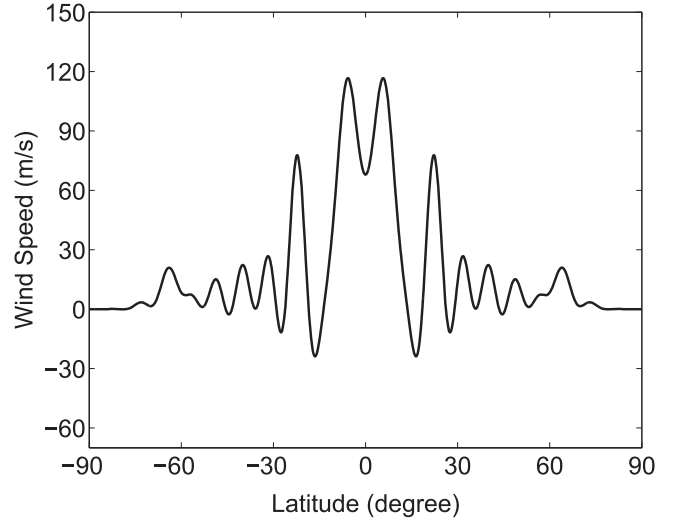


Figure 2. Latitudinal profile of the equatorially symmetric zonal winds (Porco et al. 2003) used in our calculation at the Jovian 1 bar pressure surface.

determined by the cloud-level zonal winds shown in Figure 2. It mimics the dynamically possible structure of the zonal winds confined in the domain \mathcal{D}_m under the strong rotational influence (Heimpel et al. 2005; Gastine & Wicht 2012; Jones & Kuzanyan 2012).

With the profile of the zonal winds \mathbf{u}_0 given in Figure 2 and the domain \mathcal{D}_m determined by the leading-order solution, we use a finite-element method to solve Equations (24)–(25) in the domain \mathcal{D}_m subject to the boundary condition (27) on the surfaces \mathcal{S}_m and \mathcal{S}_o . The perturbation solution $\rho'(\mathbf{r})$ is then used to calculate the external gravitational potential anomaly $V'(\mathbf{r})$. An accurate solution $V'(\mathbf{r})$ as a function of H , compared with the unprecedentedly high-precision gravitational measurements to be carried out by the *Juno* spacecraft, may help us constrain the internal structure of the zonal winds.

4. RESULTS

In discussing the results of the model, it is desirable to distinguish between two different sets of numbers/parameters. The first set, presented in Table 1, contains some parameters of Jupiter which, including the equatorial and polar radii of Jupiter R_e and R_p at the 1 bar pressure surface, are well determined by observations and, hence, can be regarded as known. The second set, including the core density ρ_c , the core equatorial radius R_c , and the density $\rho_{1 \text{ bar}}$ at the 1 bar pressure surface, is unknown, and is derived from the solution of our multi-layered model. We use the subscript *model* to denote the numbers/parameters that are obtained from the solution of the model.

We first discuss the leading-order solution of (14)–(16) subject to the conditions (17)–(18), which are characterized by the core density ρ_c , the shape \mathcal{S}_c of the core, the value of K , the shape of the 1 bar pressure surface \mathcal{S}_o , and the density profile $\rho_0(\mathbf{r})$ in the domain \mathcal{D}_o . Key characteristic values obtained from the leading-order solution are given in Table 2. The density ρ_c and the mass M_c of Jupiter’s inner core are currently unknown (Helled et al. 2011; Nettelmann et al. 2012; Hubbard & Militzer 2016). Our self-consistent solution yields a core equatorial radius $R_c = 0.09R_e$ and core density $\rho_c = 2.0 \times 10^4 \text{ kg m}^{-3}$ corresponding to $M_c = 3.73$ Earth masses, consistent with existing interior models of Jupiter (Stevenson 1982;

Table 1
The Four Parameters of Jupiter

	Observation	Model	Relative Error
M_J	$(1.8986 \pm 0.0002) \times 10^{27}$ kg	$(M_J)_{\text{model}} = 1.8986 \times 10^{27}$ kg	0.01%
R_e	71492 ± 4 km	$(R_e)_{\text{model}} = 71491$ km	0.0014%
R_p	66854 ± 10 km	$(R_p)_{\text{model}} = 66852$ km	0.0029%
Ω_J	1.75852×10^{-4} s $^{-1}$

Notes. The four parameters of Jupiter [Mass M_J (Williams 2010), equatorial radius R_e , polar radius R_p , and angular velocity Ω_J (Seidemann et al. 2010)], regarded as accurately determined by existing observations, along with the corresponding values from the solution of the leading-order problem, where the uncertainty in Jupiter's mass is computed according to the uncertainty in the gravitational constant $G = (6.67384 \pm 0.00080) \times 10^{-11}$ m 3 kg $^{-1}$ s $^{-2}$.

Table 2

Several Key Numbers/Parameters Obtained from the Leading-order Solution

Core equatorial radius (R_c)	$0.09R_e$
Core mass (M_c)	3.73 Earth masses
Core eccentricity (\mathcal{E}_c)	0.11747
Density at the core-metallic interface \mathcal{S}_c (ρ_c)	3.11423×10^3 kg m $^{-3}$
Density at the 1 bar pressure surface \mathcal{S}_o ($\rho_{1 \text{ bar}}$)	0.72737 kg m $^{-3}$
The value of K	189013.65 Pa m 6 kg $^{-2}$

Guillot 2005; Helled et al. 2011; Hubbard & Militzer 2016). Our calculation also shows that the shape of the core-metallic interface \mathcal{S}_c , because of its central location and small size, is accurately described by the oblate spheroid

$$\frac{x^2 + y^2}{R_c^2} + \frac{z^2}{R_c^2(1 - \mathcal{E}_c^2)} = 1,$$

where \mathcal{E}_c denotes the eccentricity of the spheroid and R_c is the core equatorial radius, whose values are presented in Table 2.

Our self-consistent leading-order solution reveals that the 1 bar pressure surface \mathcal{S}_o of Jupiter can be described by the equation

$$\begin{aligned} \xi_{1 \text{ bar-surface}} = & 2.63938[1 - 1.2387 \times 10^{-4} \tilde{P}_2^0(\eta) \\ & + 2.0934 \times 10^{-4} \tilde{P}_4^0(\eta) - 1.0284 \\ & \times 10^{-5} \tilde{P}_6^0(\eta) + 4.3664 \times 10^{-7} \tilde{P}_8^0(\eta)], \quad (28) \end{aligned}$$

where small higher-order terms for $\tilde{P}_n^0(\eta)$ with $n \geq 10$ are neglected with the oblate spheroidal coordinate η being defined by (19)–(21). Equation (28) describes the irregular shape of Jupiter at the 1 bar pressure surface \mathcal{S}_o which, because all the coefficients for $\tilde{P}_n^0(\eta)$ with $n \geq 2$ in (28) are much smaller than unity, deviates only slightly from an oblate spheroid. Using (28) together with (19)–(21), we find that the equatorial radius at 1 bar pressure, evaluated by letting $\eta = 1$, is $(R_e)_{\text{model}} = 71,491$ km while the polar radius, evaluated by letting $\eta = 0$, is $(R_p)_{\text{model}} = 66,852$ km; these agree with the observed values within their error bars, as shown in Table 2. Moreover, the leading-order solution also leads to the total mass of Jupiter,

$$(M_J)_{\text{model}} = \iint \int_{\mathcal{D}_c} \rho_c d^3\mathbf{r}' + \iint \int_{\mathcal{D}_o} \rho_o(\mathbf{r}') d^3\mathbf{r}',$$

which is $(M_J)_{\text{model}} = 1.8986 \times 10^{27}$ kg and, as shown in Table 2, is in agreement with the known mass M_J within its error bar.

Table 3

Gravitational Zonal Coefficients $(J_n)_0$ in the Expansion (29) Derived from the Self-consistent Leading-order Solution, Which Should be Compared with the Observed Values $(J_n)_{\text{obs}}$

n	Model $(J_n)_0 \times 10^6$	Observation $(J_n)_{\text{obs}} \times 10^6$	Relative Error
2	+14696.449	+14696.43 \pm 0.21 (Jacobson 2003)	0.00013%
4	−569.216	−587.14 \pm 1.68 (Jacobson 2003)	3.05%
6	+32.535	+34.25 \pm 5.22 (Jacobson 2003)	5.02%
8	−2.234
10	+0.150
12	−0.017

After determining the core density ρ_c in \mathcal{D}_c , the core-metallic interface \mathcal{S}_c , the 1 bar pressure surface \mathcal{S}_o , and the density profile $\rho_o(\mathbf{r})$ in \mathcal{D}_o , we can compute the external gravitational potential $V_o(\mathbf{r})$ according to

$$V_o(\mathbf{r}) = -G \left[\iiint_{\mathcal{D}_c} \frac{\rho_c d^3\mathbf{r}'}{|\mathbf{r} - \mathbf{r}'|} + \iiint_{\mathcal{D}_o} \frac{\rho_o(\mathbf{r}') d^3\mathbf{r}'}{|\mathbf{r} - \mathbf{r}'|} \right],$$

$|\mathbf{r}| \geq R_e,$

which is further expanded in terms of the zonal gravitational coefficients $(J_n)_0$:

$$V_o(\mathbf{r}) = -\frac{GM_J}{r} \left[1 - \sum_{n=2}^{\infty} (J_n)_0 \left(\frac{R_e}{r} \right)^n P_n(\cos \theta) \right], \quad r \geq R_e, \quad (29)$$

where $P_n(\cos \theta)$ is normalized such that

$$\int_0^\pi \sin \theta |P_n(\cos \theta)|^2 d\theta = \frac{2}{2n + 1}.$$

The zonal gravitational coefficients $(J_n)_0$ in (29) are then obtained by performing the following integration

$$\begin{aligned} (J_n)_0 = & -\frac{(2n + 1)R_e}{2M_J} \int_0^\pi \left[\iiint_{\mathcal{D}_c} \frac{\rho_c d^3\mathbf{r}'}{|\mathbf{r} - \mathbf{r}'|} \right. \\ & \left. + \iiint_{\mathcal{D}_o} \frac{\rho_o(\mathbf{r}') d^3\mathbf{r}'}{|\mathbf{r} - \mathbf{r}'|} \right]_{|\mathbf{r}|=R_e} \sin \theta P_n d\theta. \quad (30) \end{aligned}$$

Several values of the zonal gravitational coefficients $(J_n)_0$, up to $n = 12$, computed from the fully self-consistent solution through (30), are listed in Table 3. It can be seen that our multi-layered model is able to produce the known value of J_2 of Jupiter within its error bar along with the known gravitational

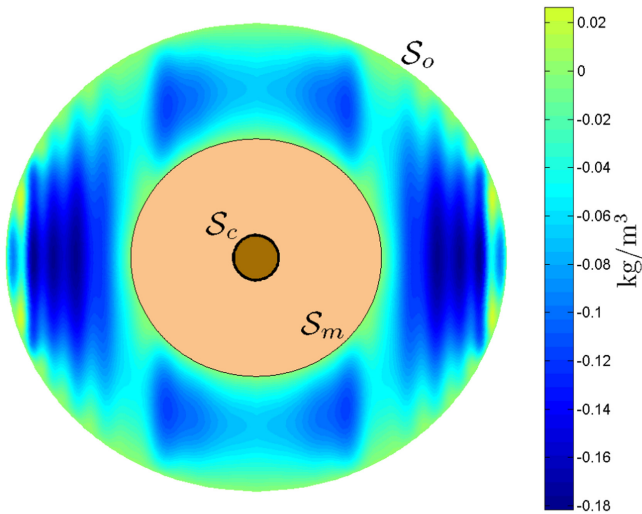


Figure 3. Density anomaly $\rho'(\mathbf{r})$ in a meridional plane caused by the zonal winds and confined between the molecular-metallic interface \mathcal{S}_m and the 1 bar pressure surface \mathcal{S}_o with $H = 0.5$.

coefficients J_4 and J_6 with about 5% accuracy. A more accurate determination of J_4 and J_6 would likely be possible with adoption of a more realistic equation of state for the molecular-metallic region. The polytrope equation of state used here is a good approximation to the real Jupiter, but an approximation nevertheless. Actually, the accuracy with which we can determine so many of Jupiter’s properties with such a simple equation of state is impressive. The analysis of this paper can be readily extended to more complex and perhaps more realistic equations of state.

We now discuss the next-order solution of Equations (24)–(25) subject to the boundary condition (27). In our model, the equatorially symmetric zonal winds (Porco et al. 2003), shown in Figure 2, are assumed to take place at the 1 bar pressure surface and extend on cylinders only through the domain \mathcal{D}_m bounded by the 1 bar pressure surface \mathcal{S}_o and the molecular-metallic interface \mathcal{S}_m ; the interface \mathcal{S}_m represents a constant density surface located between \mathcal{S}_c and \mathcal{S}_o (see Figure 1) whose equatorial radius is HR_e and whose shape is generally non-spheroidal. Since $(J_n)_0$ in (29) has already taken account of the full effect of rotational distortion, its variation, denoted by ΔJ_n and related to the solution $\rho'(\mathbf{r})$ to (24)–(25), is solely caused by the effect of the zonal winds confined within the domain \mathcal{D}_m . In computing ΔJ_n , we regard the location of the interface \mathcal{S}_m as a parameter and consider the following four cases: (1) a very deep wind profile with $H = 0.5$, (2) an intermediate deep profile with $H = 0.78$, (3) a shallow profile with $H = 0.90$, and (4) a very shallow profile with $H = 0.95$.

The density anomaly $\rho'(\mathbf{r})$ for the case $H = 0.5$ is depicted in Figure 3, showing that the maximum amplitude of the anomaly is about 0.2 kg m^{-3} in the domain \mathcal{D}_m . Modified by the boundary condition required on the surfaces \mathcal{S}_m and \mathcal{S}_o , the distribution of the density anomaly $\rho'(\mathbf{r})$ largely reflects the cylindrical structure of the zonal winds displayed in Figure 2. It should be noted that the shapes of \mathcal{S}_m and \mathcal{S}_o in Figure 3 are non-spheroidal, but their deviations from oblate spheroids are too small to be noticeable in the figure. After obtaining the density anomaly $\rho'(\mathbf{r})$ in the domain \mathcal{D}_m , we can then compute the variation ΔJ_n caused by the deep zonal winds via the

following integration

$$\Delta J_n = \frac{(2n+1)R_e}{2GM_J} \int_0^\pi \left[\int \int \int_{\mathcal{D}_m} \frac{\rho'(\mathbf{r}') d^3 \mathbf{r}'}{|\mathbf{r} - \mathbf{r}'|} \right]_{|r|=R_e} \times P_n(\cos \theta) \sin \theta d\theta. \quad (31)$$

The results, along with other cases, are presented in Table 4, revealing that, while the effect of the zonal winds on the lower-order coefficients is weak with $|\Delta J_n/(J_n)_0| \ll 1\%$ for $n = 2, 4, 6$, it becomes substantial for the high-order coefficients when $n \geq 10$. In particular, the coefficient at $n = 12$ with $|\Delta J_{12}/(J_{12})_0| \approx 300\%$ is dominated by the redistribution of mass produced by the deep zonal winds. The density anomaly $\rho'(\mathbf{r})$ in the case with $H = 0.78$ is shown in Figure 4. Compared to the density anomaly in the case with $H = 0.5$, the amplitude of the density anomaly $\rho'(\mathbf{r})$ is reduced to the maximum value of about 0.1 kg m^{-3} together with the expected cylindrical structure in the smaller domain \mathcal{D}_m . The variation of $(J_n)_0$ caused by the zonal winds with $H = 0.78$ is presented in Table 4, showing again that the effect of the zonal winds on the lower-order coefficients is weak compared to the effect of rotation, i.e., $|\Delta J_n/(J_n)_0| \ll 1\%$ for $n = 2, 4, 6$, but it becomes substantial for the high-order coefficients with $n \geq 10$.

The cases with $H = 0.9$ and $H = 0.95$ represent shallow wind models similar to that studied by direct numerical simulations (Heimpel et al. 2005). Figure 5 shows the profile of the density anomalies $\rho'(\mathbf{r})$ in the shallow, non-spheroidal-shell domain \mathcal{D}_m . There are two interesting features emerging from this shallow model. First, although the profile is still marked by cylindrical structure, the density anomaly $\rho'(\mathbf{r})$, compared to the case $H = 0.78$, has quite a different structure. Though the same zonal winds \mathbf{u}_0 in Figure 2 are adopted for all the calculations, the negative density anomaly is predominant in the case with $H = 0.78$, as displayed in Figure 4, while the positive anomaly becomes more pronounced in the case with $H = 0.90$ shown in Figure 5. It suggests that the solution $\rho'(\mathbf{r})$ to (24)–(25) is significantly influenced by the location of the interface \mathcal{S}_m where the boundary condition (27) must be satisfied. Second, the density anomaly $\rho'(\mathbf{r})$ occurs mainly in the equatorial region and makes a dominant contribution to the volume integration in (31). This would be expected since the zonal winds \mathbf{u}_0 have the largest amplitude in the equatorial region. After obtaining the density anomaly $\rho'(\mathbf{r})$ in the domain \mathcal{D}_m , we then compute ΔJ_n caused by the shallow zonal winds, the results of which are presented in Table 4. Again the effect of the zonal winds on the lower-order coefficients is found to be weak with $|\Delta J_n/(J_n)_0| \ll 1\%$ for $n = 2, 4, 6$; the coefficient at $n = 12$ still changes substantially with $|\Delta J_{12}/(J_{12})_0| \approx 235\%$ at $H = 0.90$ and $|\Delta J_{12}/(J_{12})_0| \approx 550\%$ at $H = 0.95$. An important feature is that the size of ΔJ_0 and ΔJ_{12} varies with the location of the molecular-metallic interface \mathcal{S}_m marked by the size of the parameter H .

5. SUMMARY AND REMARKS

This paper presents a fully self-consistent, multi-layered Jovian model composed of three parts: an inner core, a metallic dynamo region, and an outer molecular envelope. We have solved the governing equations for the model via a perturbation approach. The leading-order solution produces the core density ρ_c , the core-metallic interface \mathcal{S}_c , the 1 bar pressure surface \mathcal{S}_o , and the density profile $\rho_0(\mathbf{r})$ in \mathcal{D}_o . Our self-consistent solution

Table 4
Variations ΔJ_n in Zonal Gravitational Coefficients (J_n)₀, Up to $n = 12$, Caused by the Zonal Winds with $H = 0.5, 0.78, 0.90, 0.95$ on the Rotationally Distorted Non-spheroidal Jupiter

n	$(J_n)_0$	$\Delta J_n(H = 0.5)$	$\Delta J_n(H = 0.78)$	$\Delta J_n(H = 0.90)$	$\Delta J_n(H = 0.95)$
2	14696.45×10^{-6}	5.35×10^{-6}	1.99×10^{-6}	-0.05×10^{-6}	0.27×10^{-6}
4	-569.22×10^{-6}	-1.72×10^{-6}	-0.75×10^{-6}	0.12×10^{-6}	-0.19×10^{-6}
6	32.54×10^{-6}	0.25×10^{-6}	0.14×10^{-6}	-0.13×10^{-6}	0.15×10^{-6}
8	-2.23×10^{-6}	0.07×10^{-6}	-0.03×10^{-6}	0.08×10^{-6}	-0.14×10^{-6}
10	0.15×10^{-6}	0.09×10^{-6}	0.10×10^{-6}	-0.00×10^{-6}	0.13×10^{-6}
12	-0.02×10^{-6}	-0.05×10^{-6}	-0.06×10^{-6}	-0.04×10^{-6}	-0.11×10^{-6}

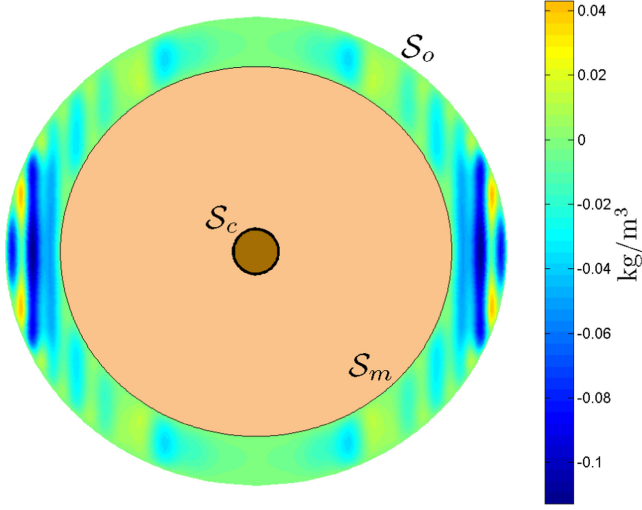


Figure 4. Density anomaly $\rho'(r)$ in a meridional plane caused by the zonal winds and confined between the molecular-metallic interface S_m and the 1 bar pressure surface S_o with $H = 0.78$.

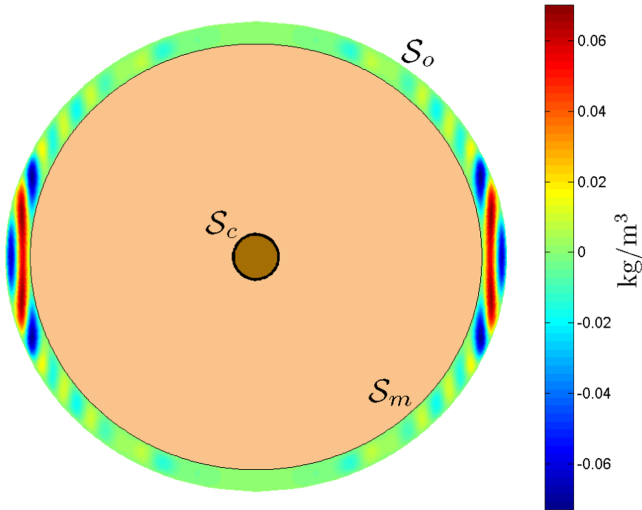


Figure 5. Density anomaly $\rho'(r)$ in a meridional plane caused by the zonal winds and confined between the molecular-metallic interface S_m and the 1 bar pressure surface S_o with $H = 0.90$.

gives rise to the core equatorial radius $R_c = 0.09R_e$ with its mass corresponding to 3.73 Earth masses. The next-order problem determines the variation of the Jovian gravitational field caused solely by the effect of the zonal winds on the rotationally distorted non-spheroidal Jupiter. In our multi-layered model, the zonal winds are assumed to be on cylinders parallel to the rotation axis, but confined between the 1 bar

pressure surface S_o and the molecular-metallic interface S_m , and the location of the interface S_m is treated as a model parameter. Compared to the single-layer, spheroidal model (Kong et al. 2013a, 2013b), the fully self-consistent, multi-layered model, even though mathematically and numerically much more complicated, is more realistic and accurate, particularly for the high-degree gravitational coefficients of Jupiter.

It is anticipated that the ongoing *Juno* spacecraft will achieve high precision in its determination of the gravitational field with the relative uncertainty 10^{-9} (Kaspi et al. 2010). An accurate fully self-consistent, multi-layered Jovian model would enable an important constraint on the depth and structure of the zonal winds of Jupiter. In this connection, the dependence of the high-degree coefficients such as J_{10} and J_{12} on the location of the molecular-metallic interface, which is presented in Table 4, may provide a way of probing or constraining the structure of the zonal winds.

Our multi-layered model, because of the adoption of a single equation of state for both the molecular and metallic envelopes in Jupiter, cannot make a more accurate determination of higher-order gravitational coefficients such as J_4 . The model can be extended by introducing two different polytropic equations of state, $p = K_{\text{molecular}}\rho^2$ and $p = K_{\text{metallic}}\rho^2$, for the metallic and the molecular envelopes respectively. With the two polytropic equations of state, the coupled multi-layered system would become mathematically more complicated and computationally more difficult to solve but can be, in principle, used to reproduce the value of J_4 . Generally speaking, although using the same polytropic equation of state for both the molecular and metallic envelopes (which is mathematically and computationally convenient) offers a reasonably good approximation to the real Jupiter, a more realistic equation of state is required in order to reproduce the observed values of the higher-order coefficients J_4 and J_6 .

Density at the 1 bar pressure surface, $\rho_{1 \text{ bar}}$, of Jupiter can be estimated by using an ideal H/He gas at 1 bar with temperature $T = 165$ K and a He mass fraction of about 0.238, as suggested by the Galileo entry probe. This estimation gives rise to $\rho_{1 \text{ bar}} \approx 0.2 \text{ kg m}^{-3}$, which is smaller than $\rho_{1 \text{ bar}} \approx 0.7 \text{ kg m}^{-3}$ derived from our present model. This disagreement would be expected and is a consequence of the simplistic equation of state adopted in our model, just as our inability to match higher-order gravitational coefficients J_4 and J_6 . If we had a more realistic equation of state with more parameters, we could specify the 1 bar density $\rho_{1 \text{ bar}}$ as a constraint to be satisfied just as we satisfy other quantities. In other words, the present simplistic equation-of-state model can be improved in the future by employing a more realistic equation of state—which in turn constrains the form of equation of state for the Jovian interior through the structure of its gravitational field.

An introduction of the location of the molecular-metallic interface \mathcal{S}_m in the multi-layered model represents a significant advantage in constraining the structure of the zonal winds. This is because the cloud-level zonal winds are unlikely to extend all the way on the cylinders, particularly in higher latitudes, from the northern to southern atmosphere without being hindered by the Jovian convective dynamo (Liu et al. 2008). It follows that, when probing the deep structure of the zonal winds, a depth parameter needs to be introduced in the model of Jovian gravitational sounding. One possible way is to introduce the radially decaying factor H_r (Kaspi et al. 2010) in the form

$$\mathbf{u}_0 \sim e^{-\left(\frac{R_e-r}{H_r}\right)}.$$

However, according to the well-known theory of rotating fluid dynamics (Chandrasekhar 1962) and the known result of rotating convection and dynamo simulations (Zhang & Schubert 2000; Heimpel et al. 2005; Gastine & Wicht 2012; Jones & Kuzanyan 2012), the zonal winds \mathbf{u}_0 are likely, even in the presence of stratified layers, to extend on cylinders parallel to the rotation axis but cannot penetrate into the metallic dynamo region because of magnetic braking. In other words, the cylindrical structure confined in \mathcal{D}_m and the location parameter H in our multi-layered model (the size of H actually provides a measure of the unknown size of the Jovian dynamo region) reflect not only the possible internal structure of Jupiter, but also the correct dynamics controlled by the effect of its rapid rotation.

A direct comparison of our present results and those of Kaspi et al. (2010; referred to as the other model below) is uninformative because of the following reasons. First, our model has non-spherical, multi-layered geometry and is able to produce the known mass, the known equatorial and polar radii, and the known coefficient J_2 of Jupiter within their error bars, while the other model is spherical and single-layered. Second, our model is mathematically marked by a unique solution of the well-defined equations satisfying the appropriate boundary conditions while the other model is based on the thermal-wind equation that merely represents a diagnostic relation, i.e., it does not have a unique solution and does not require any boundary condition. Third, the thermal-wind equation should be generalized to account for an associated gravitational perturbation (Zhang et al. 2015), which results in the thermal-gravitational wind equation, a two-dimensional kernel

integral equation with the Green's function in its integrand, whose mathematical and physical properties are poorly understood.

K.Z. is supported by Leverhulme Trust Research Project Grant RPG-2015-096 and by Macau FDCT grants 039/2013/A2 and 007/2016/A1. The computation made use of the high performance computing resources in the Core Facility for Advanced Research Computing at Shanghai Astronomical Observatory, Chinese Academy of Sciences.

REFERENCES

- Bolton, S. J. 2005, Juno Final Concept Study Report Tech. Rep. AO-03-OSS-03 (Washington, DC: NASA)
- Chandrasekhar, S. 1962, *Hydrodynamic and Hydromagnetic Stability* (Oxford: Clarendon)
- Gastine, T., & Wicht, J. 2012, *Icar*, **219**, 428
- Guillot, T. 2005, *AREPS*, **33**, 493
- Heimpel, M., Aurnou, J. M., & Wicht, J. 2005, *Natur*, **438**, 193
- Helled, R., Anderson, J. D., Schubert, G., & Stevenson, D. J. 2011, *Icar*, **216**, 440
- Hubbard, W. B. 1999, *Icar*, **137**, 357
- Hubbard, W. B. 2013, *ApJ*, **768**, 43
- Hubbard, W. B., & Militzer, B. 2016, *ApJ*, **820**, 80
- Hubbard, W. B., Schubert, G., Kong, D., & Zhang, K. 2014, *Icar*, **242**, 138
- Jacobson, R. A. 2003, JUP 230 Orbit Solution, http://ssd.jpl.nasa.gov/?gravity_fields_op
- Jones, C. A., & Kuzanyan, K. M. 2012, *Icar*, **204**, 227
- Kaspi, Y., Hubbard, W. B., Showman, A. P., & Flierl, G. R. 2010, *GeoRL*, **37**, L01204
- Kong, D., Liao, X., Zhang, K., & Schubert, G. 2013a, *Icar*, **226**, 1425
- Kong, D., Liao, X., Zhang, K., & Schubert, G. 2014, *ApJL*, **791**, L24
- Kong, D., Zhang, K., & Schubert, G. 2015, *PEPI*, **249**, 43
- Kong, D., Zhang, K., & Schubert, G. 2016, *NatSR*, **6**, 23497
- Kong, D., Zhang, K., Schubert, G., & Anderson, J. 2013b, *ApJ*, **763**, 116
- Liu, J., Goldreich, P. M., & Stevenson, D. J. 2008, *Icar*, **196**, 653
- Nettelmann, N., Becker, A., Holst, B., & Redmer, R. 2012, *ApJ*, **750**, 52
- Porco, C. C., West, R. A., McEwen, A., et al. 2003, *Sci*, **299**, 1541
- Seidelmann, P. K., Abalakin, V. K., Bursa, M., et al. 2001, Report of the IAU/ IAG Working Group on Cartographic Coordinates and Rotational Elements of the Planets and Satellites: 2000, HNSKY Planetarium Program, <http://www.hnsky.org/iau-iag.htm>
- Seidelmann, P. K., Archinal, B. A., A'hearn, M. F., et al. 2007, *CeMDA*, **98**, 155
- Stevenson, D. 1982, *AREPS*, **10**, 257
- Williams, D. R. 2010, Jupiter Fact Sheet, <http://nssdc.gsfc.nasa.gov/planetary/factsheet/jupiterfact.html>
- Zhang, K., Kong, D., & Schubert, G. 2015, *ApJ*, **806**, 270
- Zhang, K., & Schubert, G. 2000, *Sci*, **290**, 1944